Geophysical Research Letters

RESEARCH LETTER
10.1029/2018GL078133

Key Points:
- Surface temperatures below the Vostok record low 2-m air temperature are observed at multiple sites near the East Antarctic ice divide
- Lowest surface temperatures, ~−98 °C, are in high-elevation shallow topographic depressions, with inferred 2-m air temperatures of ~−94 ± 4 °C
- Clear-air downwelling thermal emission and heat conduction from subsurface snow appear to control the low-temperature limit

Supporting Information:
- Supporting Information S1
- Figure S1

Correspondence to:
T. A. Scambos,
teds@nsidc.org

Citation:
Scambos, T. A., Campbell, G. G., Pope, A., Haran, T., Muto, A., Lazzara, M., et al. (2018). Ultralow surface temperatures in East Antarctica from satellite thermal infrared mapping: The coldest places on Earth. *Geophysical Research Letters*, *45*, 6124–6133. https://doi.org/10.1029/2018GL078133

Received 28 MAR 2018
Accepted 29 MAY 2018
Accepted article online 25 JUN 2018
Published online 29 JUN 2018

Ultralow Surface Temperatures in East Antarctica From Satellite Thermal Infrared Mapping: The Coldest Places on Earth

T. A. Scambos[1], G. G. Campbell[1], A. Pope[1], T. Haran[1], A. Muto[2], M. Lazzara[3], C. H. Reijmer[4], and M. R. van den Broeke[4]

[1]National Snow and Ice Data Center, University of Colorado at Boulder, Boulder, CO, USA, [2]Department of Earth and Environmental Science, Temple University, Philadelphia, PA, USA, [3]Antarctic Meteorological Research Center, University of Wisconsin-Madison and Madison Area Technical College, Madison, WI, USA, [4]Institute for Marine and Atmospheric Research, Utrecht University, Utrecht, Netherlands

Abstract We identify areas near the East Antarctic ice divide where <−90 °C surface snow temperatures are observed in wintertime satellite thermal-band data under clear-sky conditions. The lowest temperatures are found in small (<200 km^2) topographic basins of ~2 m depth above 3,800 m elevation. Approximately 100 sites have observed minimum surface temperatures of ~−98 °C during the winters of 2004–2016. Comparisons of surface snow temperatures with near-surface air temperatures at nearby weather stations indicate that ~−98 °C surfaces imply ~−94 ± 4 °C 2-m air temperatures. Landsat 8 thermal band data and elevation data show gradients near the topographic depressions of ~6 °C km^{-1} horizontally and ~4 °C m^{-1} vertically. Ultralow temperature occurrences correlate with strong polar vortex circulation. We discuss a conceptual model of radiative surface cooling that produces an extreme inversion layer. Further cooling occurs as near-surface cold air pools in shallow high-elevation topographic basins, moderated by clear-air downwelling radiation and heat from subsurface snow.

Plain Language Summary The lowest measured air temperature on Earth is −89.2 °C (−129 F) on 23 July 1983, observed at Vostok Station in Antarctica (Turner et al., 2009, https://doi.org/10.1029/2009JD012104). However, satellite data collected during the Antarctic polar night during 2004–2016 reveal a broad region of the high East Antarctic Plateau above Vostok that regularly reaches snow surface temperatures of −90 °C and below. These occur in shallow topographic depressions near the highest part of the ice sheet, at 3,800 to 4,050-m elevation. Comparisons with nearby automated weather stations suggest that air temperatures during these events are near −94 ± 4 °C or about −138 F. Ultracold conditions (below −90 °C) occur more frequently when the Antarctic polar vortex is strong. This temperature appears to be about as low as it is possible to reach, even under clear skies and very dry conditions, because heat radiating from the cold clear air is nearly equal to the heat radiating from the bitterly cold snow surface.

1. Introduction

Extremely low air and surface temperatures occur in East Antarctica, caused by intense radiative cooling of the snow surface during prolonged wintertime periods of clear sky, weak winds, and very dry atmosphere (Turner et al., 2009). Dry snow exhibits high emissivity in the thermal wavelength range (ε = 0.997 over 8 to 14 μm; Dozier & Warren, 1982), particularly the very fine-grained acicular snow typical of the East Antarctic Plateau (ε = 0.999 at 10 to 11 μm; Salisbury et al., 1994). Chilling of the air layer immediately above the snow surface by contact with the radiatively cooling snow leads to a strong thermal inversion in the lowest few meters of the atmosphere (Hudson & Brandt, 2005; Phillpot & Zillman, 1970; Scambos et al., 2006). The resulting increased density of this air layer and the regional surface slope of the ice sheet drive katabatic airflow across the entire continent (Parish & Bromwich, 1987) at speeds depending on both local and regional slope, as well as additional synoptic and thermal pressure gradients (van den Broeke & van Lipzig, 2003). This airflow, if it becomes partly or wholly turbulent, can disrupt the near-surface temperature inversion, warming the surface by sensible heat exchange. A steep thermal gradient is also produced in the near-surface snow and firn layer by the surface radiative cooling (King et al., 1996; Weller & Schwerdtfeger, 1977), driving intense vapor transport and recrystallization in the upper snow layers (Albert et al., 2004).

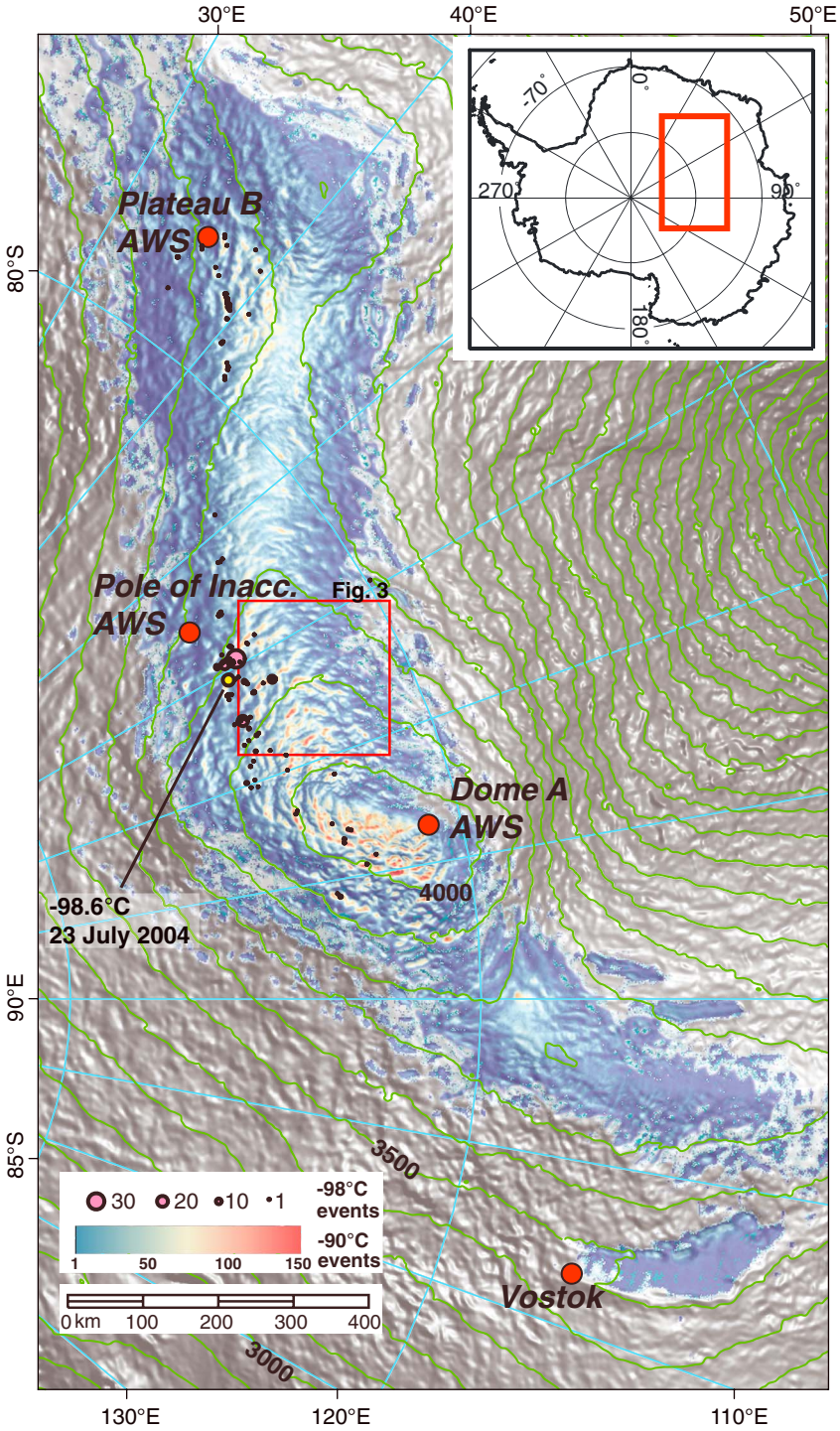

Figure 1. The shaded relief map of the Dome Fuji-Dome Argus region of the East Antarctic Plateau with red-yellow-blue color scale indicating occurrences of thermal emission surface temperatures <−90 °C in the Moderate Resolution Imaging Spectroradiometer (MODIS) MYD11 data set. Elevation data are from a digital elevation model (Bamber et al., 2009). The small circles indicate ~100 regions where observed temperatures of <−98 °C have occurred, with circle size scaled to number of occurrences. The red box shows area of Landsat 8 Thermal Infrared Sensor/Aqua MODIS LST comparison region shown in Figure 3.

Extensive literature has described the formation of temperature inversions over ice sheets (Hudson & Brandt, 2005; Phillpot & Zillman, 1970), but only a few studies describe the meteorology and other conditions of the very coldest events (Stepanova, 1963; Turner et al., 2009). An earlier study identified the highest surface temperatures on Earth (three sites are essentially tied, two in Iran, and one in Algeria; Mildrexler et al., 2006), but concerns about cloud contamination limited attempts to identify record low temperature sites from satellite data over ice sheets. The recognition here that the coldest Antarctic conditions occur under a clear atmospheric column allows us to explore the climate, geography, and near-surface conditions of the coldest places on Earth.

2. Methods and Data

Satellite-derived thermal emission temperature data from Moderate Resolution Imaging Spectroradiometer (MODIS) Land Surface Temperature data (LST); both MOD11 (from Terra) and MYD11 (from Aqua) data sets were used to evaluate the location and frequency of very low temperatures in Antarctica (Figure 1 and Figure S1a in the supporting information). A pilot study using Advanced Very High Resolution Radiometer data confirmed the general locations and value of very low surface temperatures (Figure S1b; Wang & Key, 2005). We extracted minimum temperatures in the LST satellite swath data south of 70°S (gridded to a 1-km polar stereographic projection) between 15 June to 15 September for a 12-year period (2004–2016; MOD11 Collection 6 and MYD11 Collections 5 and 6; Wan, 2006; Wang et al., 2013). The 2004 winter was the earliest MODIS Collection 6 data available at the time we began our analysis. We used the LST cloud mask, although this by itself is only partially effective. Terra MOD11 Collection 5 (hereafter, MOD11 c5) does not contain surface temperatures below 200 K (−73.15 °C) because they were assumed to be cloud-contaminated. This was adjusted in MOD11 c6. Aqua MYD11 reports lower temperature values in c5 because problems with the Aqua MODIS band 6 (1,640 nm) compromised high cloud detection. The Terra MOD11 cloud mask, using a functioning band 6, also masked clear-sky observations of very low surface temperatures. The Aqua MYD11 masking protocol did not mask observations of the lowest surface temperatures (Gladkova et al., 2013), and we show that many of these are cloud-free (Figures S1 and S2). Initial assessments using MYD11 c5 data produced results similar to MOD11 c6, but masking of temperatures below 180 K (−93.15 °C) in MYD11c5 eliminated the very lowest values.

The extracted grids of minimum 1982–2000 and 2004–2016 temperatures (Advanced Very High Resolution Radiometer and MODIS) reveal that above ~3,250-m elevation, the spatial pattern of the lowest temperatures represents an image of the local surface topography interacting with the near-surface air inversion and is not perceptibly obscured or modified by cloud thermal patterns. This was confirmed by comparison with the visible-band MODIS Mosaic of Antarctica (MOA2009; Haran et al., 2014) and a satellite-derived digital elevation model (Bamber et al., 2009; Figure S2). The high correlation with surface morphology indicates that the lowest temperatures occur under clear-sky conditions and are colder than any discernible clouds (Campbell et al., 2013).

The lowest surface snow temperature in the MYD11 and MOD11 c6 data spanning 2004–2016 is −98.6 °C (Figure 2a: 22 July 2004; 82.07°S, 60.72°E). However, temperatures ranging between −98.0 °C and −98.6 °C were recorded at ~100 sites during the study period (MYD11 c6 data; Figure 1). Elevation and minimum surface temperature profiles in the region of the cold sites show that the highest number of ultralow temperature observations (<−90 °C) and the lowest observed temperatures (to <−98 °C) lie in shallow topographic basins (Figures 1 and S2 and S3).

Adjacent sites and adjacent grid cells for a single cold event show very similar time series sequences of surface snow temperature, indicating that the results are not spurious in space or time or highly dependent on one sensor or processing version (Figures 2 and S4). Observed cooling rates of the surface during ultracold events slow markedly as the surface reaches temperatures surpass −90 °C (Figures 2 and S4); they never exceed 0.4 °C/hr (averaged over 6-hr intervals) during events of 2004, 2010, and 2015 (8 different days, 25+ different sites). Typical values were 0.2 °C/hr. In some cases surface temperatures hovered between −92 and −95 °C (observed LST temperature) for more than 24 hr. Smooth variation of the time series grid cell data demonstrates again that the atmosphere in our selected satellite observations is cloud-free.

3. Comparison With In Situ Temperature Data

The record lowest 2-m air temperature, −89.2 °C, was observed at Vostok Station, Antarctica (−78.45°S, 106.83°E, 3,488 m above sea level) on 21 July 1983 (Turner et al., 2009). The minimum 2-m air temperature

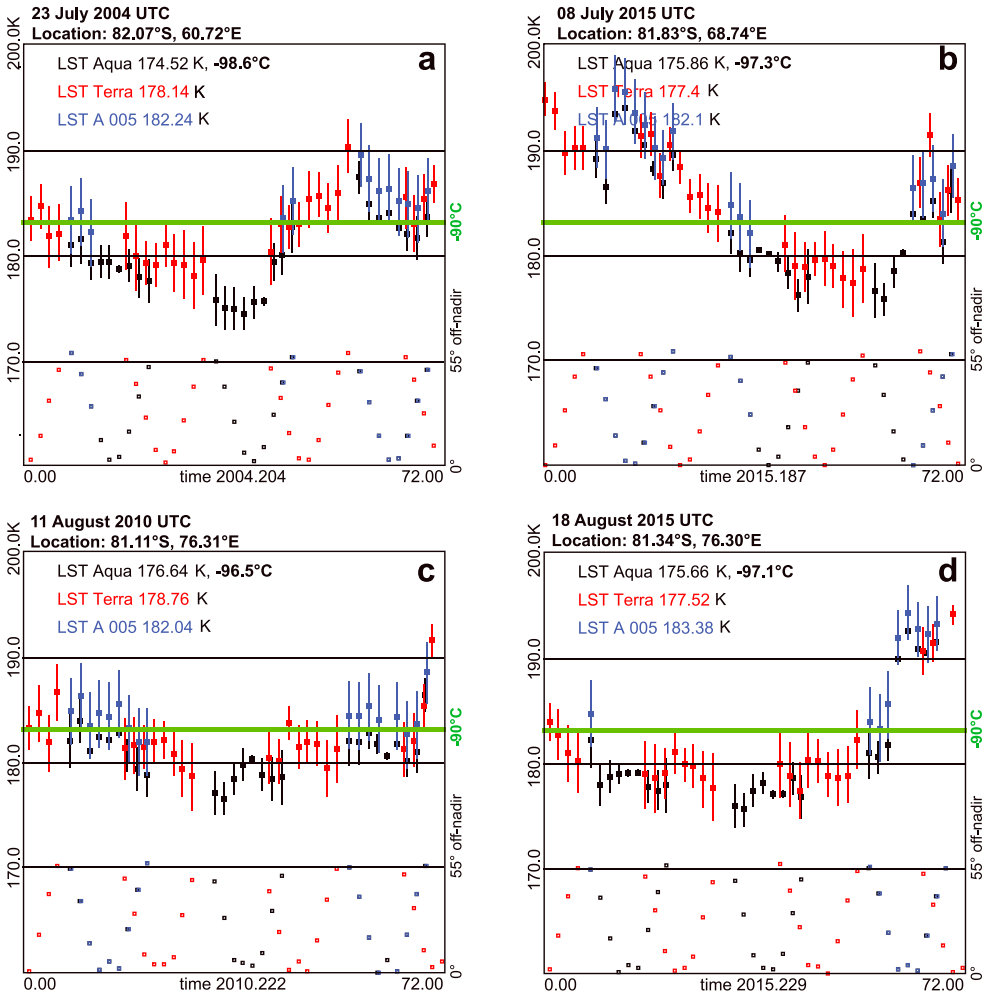

Figure 2. Moderate Resolution Imaging Spectroradiometer (MODIS) Land Surface Temperature (LST) time series data for single grid cells from swath data for selected ultracold events on the East Antarctic Plateau. (top) MODIS LST grid cell time series of surface temperature versus time in hours. "LST A 005" refers to MYD11 c5 data in the panels; the other data are LST c6. (bottom) Off-nadir viewing angle for the MODIS LST swaths. The error bars for the LST data set are based on viewing parameters and estimated water vapor in the view path.

at Vostok during our 2004–2016 LST data analysis period occurred on 15 September 2012, at −83.3 °C. Four surface snow temperature events of <−90 °C have been observed in the region during the 2004–2016 compilation, always at the opposite end (northwest) of Subglacial Lake Vostok from the air temperature observation site. Automated weather stations (AWS) located in the Dome A-Dome F region of East Antarctica have not recorded air temperatures below −85 °C. However, several of these AWS units are not operational in midwinter conditions. An examination of their locations shows that none of the AWS within the band of −90 °C surface snow temperature occurrences in Figure 1 coincide with the coldest event sites (<−98 °C).

Validation studies of MODIS c5 and c6 LST for nonpolar regions, while limited, suggest that the surface temperature data are generally within 1 °C of the in situ measured thermal emission temperature (Wan, 2014), although the validation did not extend to this temperature range or surface type. The main intent of the LST c6 reprocessing was improvement of high-temperature desert measurements. The reprocessing sought to retain the performance of c5 for lower temperatures (Wan, 2014). A recent assessment of the accuracy of MODIS LST c5 and c6 at the summit of the Greenland ice sheet (Adolph et al., 2018) found a very small bias in c6 data (−0.4 ± 0.9 °C for cloud-filtered data) in the −5 to −35 °C surface temperature range using an in situ

Table 1
Winter Air Temperature[a] and Surface Snow Temperature[b] Measurements 2008–2015

	Vostok 78.45°S, 106.83°E 3,488 m 2008–2015	Plateau B 78.65°S, 35.64°E 3,620 m 2008–2015	Pole inacc. 82.11°S, 55.03°E 3,730 m 2008–2015	Dome A 80.37°S, 77.37°E 4,084 m High	2008–2014	Low
Air temperature mean height, m	2.0	4.08	4.13	3.42	1.42	0.42
Air temperature height range, m	—	(4.4–3.7)	(4.4–3.7)	(3.6–3.1)	(1.6–1.1)	(0.59–0.09)
Lowest air temperature[c]	−83.3	−84.1	−84.6	−77.0	−78.3	−79.1
Lowest surface temperature[d]	−85.1	−89.9	−88.3	−88.0	−88.0	−86.8
Mean air temperature, °C						
During MODIS Aqua passes	−74.1 (171)	−74.3 (1,736)	−74.2 (2,942)	−68.4 (1,999)	−70.3 (2,507)	−73.5 (1,589)
During MODIS Terra passes	−73.8 (163)	−73.6 (916)	−72.9 (1,159)	−68.5 (1,312)	−70.4 (1,604)	−73.3 (1,630)
Mean LST temperature, °C						
During MODIS Aqua passes	−78.2	−79.9	−79.1	−78.4	−78.9	−78.1
During MODIS Terra passes	−76.9	−77.8	−76.8	−76.5	−76.5	−76.5
Mean air—LST gradient[e], °C m^{-1}						
AWS-MODIS Aqua	2.05	1.36	1.21	2.92	6.06	10.95
AWS-MODIS Terra	1.52	1.03	0.93	2.34	4.30	7.62

[a]Extracted from Automated weather stations (AWS) and station data, 15 June to 15 September, for air temperatures <-70 °C (<-60 °C for Dome A), wind speeds <4 ms^{-1}, and Land Surface Temperature (LST) temperatures $<$ air temperatures. Hourly temperatures from AWS, 6-hourly temperatures from Vostok station. Air temperature measurements for Plateau B and Pole of Inaccessibility AWS were calibrated prior to installation to ±0.2 °C over −30 to −90 °C. [b]LST temperatures from LST c6 data with $<\pm1$ °C error acquired within 45 min of air temperature at weather data sites. [c]Lowest temperature within the filtered weather station data having a $<\pm1$ °C error MODIS overpass within 45 min. [d]Lowest LST temperature within 45 min of air temperatures from MYD11 and MOD11 c6 swath data at weather data sites. [e]Mean offset at 2 m for the selected LST and AWS data is 4.6 °C; 1σ error for the 2-m offset is ±3.3 °C. LST error is selected to be $<\pm1$ °C. [f]Dome A AWS has three air temperature sensors. All three AWS measure snow height, which was interpolated to daily values.

infrared surface snow temperature measurement for comparison. The bias did not have a trend with observed temperature. The root mean square error range around this bias trend was ±1.0 to ±1.8 °C.

To approximately validate the ultralow LST temperatures, we compared a subset of LST surface temperatures with 2 to 4-m air temperatures at Vostok Station and three AWS that consistently operate through the winter season (Plateau B AWS, 78.650°S, 35.633°E, 3,620 m; Pole of Inaccessibility AWS, 82.167°S, 55.033°E, 3,730 m; and Dome A AWS, 80.367°S, 77.367°E, 4,084 m; Table 1). We also determined the near-surface vertical air temperature gradients at the Dome A AWS from 4, 2, and 1 m (nominal height) air temperatures (Table S1 in the supporting information). Weather station data were selected for cold midwinter conditions (15 June to 15 September; <-70 °C; for Dome A, <-60 °C) and low wind speeds (<4 ms^{-1}). We excluded cases where LST values were higher than the air temperature. In general, this combination of conditions occurs under clear skies. We further filtered the weather data to include those with a LST swath image measurement within 45 min of the air temperature acquisition and having a LST c6 reported error of <1 °C (as a further indication of a clear atmosphere and a good observational geometry). The difference between air temperatures in the lowest 2 to 4 m and local surface snow temperatures under cold conditions is approximately 1 to 2 °C m^{-1}, except for Dome A AWS where the mean gradient is 2 to 11 °C m^{-1} for the multiple air temperature sensor heights (~4.4 to 0.1 m; Tables 1 and S1).

The air temperature profile can be used as an independent estimate of surface temperature for comparison with LST temperatures, assuming that at the exact surface, air temperature and snow temperature are identical. Although the data show that the vertical temperature profile can be significantly nonlinear, it is highly variable, primarily in the last few decimeters. We use a linear extrapolation to arrive at a surface (0 m) air temperature estimate (Table S1). The weighted mean linear air-to-surface air temperature gradient in the lowest ~3.4 m is 2.7 °C m^{-1}, ranging between 1.8 and 3.7 °C m^{-1}. Comparing a surface temperature extrapolated from the mean air temperature gradient to the LST surface thermal emission temperatures under similar conditions (Table 1, Dome A values) indicates that the MODIS-based LST c6 data are approximately 0.4 °C to 2.8 °C lower than the extrapolated air temperature. Given the uncertainty of this estimate, and the wide range of possible near-surface air temperature gradients, and the selected LST error of $<\pm1$ °C, we estimate the MODIS LST data offset to be −0.5 °C (Terra LST c6) to −3.0 °C (Aqua LST c6) from surface temperature, with an estimated error of ±2.1 °C.

Examining the air temperature gradients and the air-LST differences for the four sites (Tables 1 and S1), Dome A has a stronger near-surface air temperature inversion than the AWS sites on the flanks of the East Antarctic Plateau. This characteristic of ice dome summits has been noted previously (Phillpot & Zillman, 1970; Shuman et al., 2014). We can infer that ~2-m air temperatures at the AWS sites, and across the region, are typically 4.6 (~1.5 to 5) ± 3.3 °C higher than the LST-measured surface temperature (selected for <±1 °C error; Table 1). This is similar to results from other ice sheet sites or sea ice surfaces (Hall et al., 2008; Hudson & Brandt, 2005; Scambos et al., 2006; Schwerdtfeger, 1970). Our estimate is hampered by not having actual measured air temperature gradients at other East Antarctic high-altitude stations. However, we infer that the lowest thermal-band surface snow temperatures observed in the ultracold sites in Figure 1, −98 °C to −98.6 °C, imply 2-m air temperatures of −94 ± 4 °C if the vertical air temperature gradients are similar to the three off-summit weather stations (i.e., less than Dome A, as the data suggest). Given that the coldest sites are all in shallow topographic depressions, it is possible that their near-surface air temperature gradients are lower than typical flank or dome sites, since air drainage is reduced.

4. Results

Figure 1 shows that a broad area along the main ice divide of the East Antarctic Plateau above ~3,500 m has had midwinter surface snow thermal emission temperatures (as measured by MODIS LST) below −90 °C as often as 150 times over the 2004–2016 study period. Sites of frequent −90 °C and lower temperatures are always flat or shallow depressions (few meters of closure) on the flanks of the ice divide (Figures 1, S2, and S3). The lowest temperature observed in the data set is −98.6 °C, on 23 July 2004. Several small (~10 to 200 km^2) closed basins near the Pole of Inaccessibility have up to thirty −98 °C events in the 2004–2016 LST record. However, ~100 distinct sites (separate clusters of grid cells) in our 2004–2016 compilation show reported surface temperatures of −98 °C or less. With our estimated error and analysis of the near-surface air temperature gradient, this implies that a large number of sites have reached approximately −94 ± 4 °C air temperatures at 2 m above the surface, in some cases, more than 10 times.

Surface snow temperature patterns near the region of very low temperatures were examined in greater spatial detail using Landsat-8 Thermal Infrared Sensor (TIRS) data (Roy et al., 2014; Figure 3). Forty-six TIRS images covering the East Antarctic Dome A to Dome F region (the East Antarctic ice divide) were acquired during the 2013, 2014, and 2015 austral winters. TIRS produces gridded thermal image data at ~100-m spatial resolution and 12-bit radiometric resolution. Calibration of TIRS is still ongoing, and there are several issues with the sensor (we used data corrected by the processing described in Gerace & Montanaro, 2017). We used the TIRS 10-μm sensor (band 10) as a relative thermal emission temperature mapper only, calibrating the reported thermal radiances to temperatures that regionally matched MODIS LST data.

The MODIS-adjusted TIRS data indicate that very strong thermal gradients exist at the boundaries of ultracold pocket areas (>6 °C km^{-1} horizontally; >4 °C m^{-1} vertically, using Bamber et al., 2009 DEM, and airborne elevation profiles from Bell et al., 2011). The TIRS data also reveal that the cold pocket areas have a more uniform low temperature (±1 °C) across the topographic lows (5 to 15 km across) than seen in MODIS LST data. Thermal gradients are largest on the uphill sides of the topographic depressions (Figures 3c and 3d and S3).

The total areal extent of very low surface temperatures on the East Antarctic Plateau is observed to vary greatly from year to year in our 2004–2016 winter months data set. We summed the total LST grid cell areas that reached −83 °C or below and −90 °C or below for July and August over the study period. The years with the highest total area for these temperature ranges were 2004, 2008, and 2015, with ~250 to 310 × 10^3 km^2 d reaching −83 °C or below each month in each those years and up to 22 × 10^3 km^2 d reaching −90 °C or below. The years 2007, 2009, and 2011 had very low totals, less than 20 × 10^3 km^2 d of −83 °C or below, and just a few grid cells (<50) at −90 °C or lower. Comparing the July and August daily area totals with the strength of the Southern Annular Mode (SAM) circulation index (Marshall, 2003; Marshall & National Center for Atmospheric Research Staff, 2016) revealed a strong positive correlation for both temperature levels (r = ~0.7; Figure S5). A high positive SAM index indicates a strong circum-Antarctic circulation and less intrusion of lower-latitude air masses.

The region containing the ~100 sites of the lowest temperatures (−98 °C to −98.6 °C as observed in LST; Figure 1) is 900 km long and 100 km wide, on the south side of the main East Antarctic ice divide between

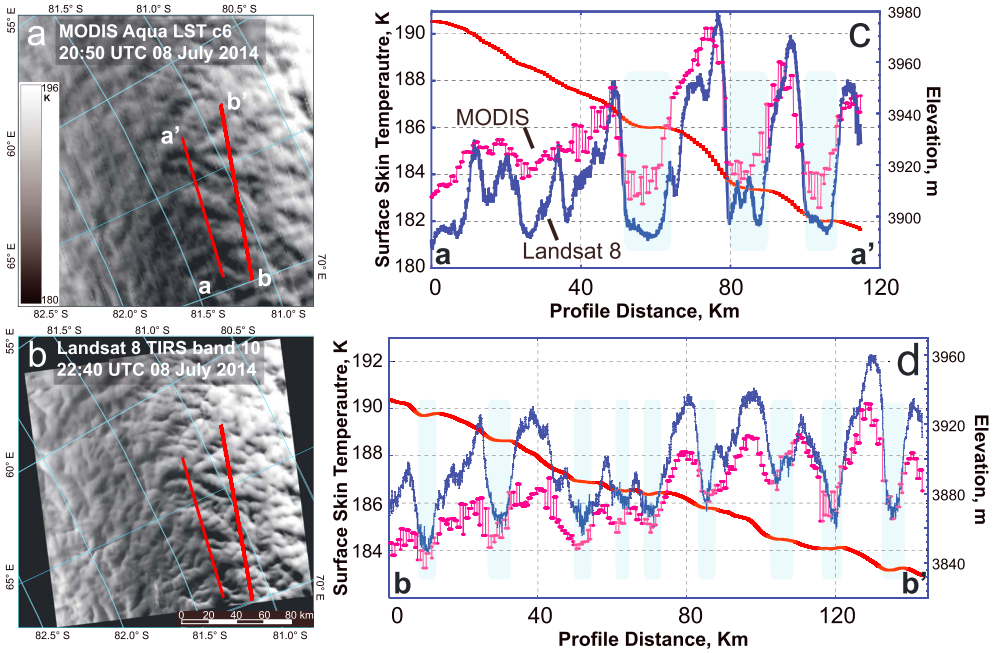

Figure 3. Comparison of (a) midwinter Aqua Moderate Resolution Imaging Spectroradiometer (MODIS) Land Surface Temperature (LST) c6 and (b) Landsat 8 Thermal Infrared Sensor band 10 image data adjusted to match MODIS LST regionally, under clear sky and low temperature conditions; (c and d) MODIS LST (pink line) and Landsat 8 TIRS (blue line) temperatures and elevation (red line) profiles (a-a′ and b-b′ in image panels; elevation for a-a′ from Bamber et al., 2009; for b-b′, Bell et al., 2011). The light blue shaded regions mark areas of flat or reverse slope.

3,850 and 4,050-m elevation. The narrow range of minimum temperatures over so large an area suggests that there is a physical control such as an external physical or atmospheric condition that restricts the minimum possible surface temperature. We consider two possibilities that may account for this. One control may be optically thin stratospheric clouds, which could limit radiative cooling rates of the surface when present, but would be absent during the coldest observations (since a cloud-free surface is visible in the lowest-temperature thermal data). A second potential limiting factor is reduced net radiative cooling of the surface as the low-temperature thermal emission spectrum is increasingly affected by absorption bands from CO_2 and water vapor outside the main atmospheric thermal emission window (7 to 13 μm).

Laser-based observations from CALIPSO data (Cloud-Aerosol Lidar and Infrared Pathfinder Satellite Observations) measure the spatial and temporal distribution of polar stratospheric clouds (PSCs) and can be used to distinguish between various types of aerosols and clouds in PSC layers (Pitts et al., 2009; Pitts & Poole, 2015). PSCs are widespread over the continent during Antarctic winter. Between late June and the end of July, PSCs can cover an area equal to the size of the Antarctic ice sheet (~8 to 18 × 10^6 km^2), approximately centered on the South Pole. Monthly mean cloud fractions in the study area for July and August from CALIPSO high-cloud assessments are ~0.30. However, optical thickness (and thermal opacity) is primarily controlled by the presence of stratospheric ice clouds, which constitute a fraction of PSCs. Ice PSC cloud fractions are 0.05 to 0.15 for 2006–2014 and have an opacity of 0.4 to 0.9 (Pitts et al., 2009; Pitts & Poole, 2015). Atmospheric profiles for the East Antarctic troposphere and stratosphere from balloon-borne rawinsonde data from Amundsen-Scott South Pole Station (https://www.esrl.noaa.gov/gmd/dv/spo_oz/movies/index.html) indicate that the annual minimum temperature in the upper atmosphere (18 to 23 km) is ~−92 to −95 °C and is typically reached in middle to late July. CALIPSO observations show that the minimum observed temperature of PSCs is ~−90 °C (Pitts et al., 2009). These temperatures are similar to or slightly above our estimate of the corrected minimum surface temperatures for the −98 °C LST observations. Ice clouds as observed by CALIPSO would likely constrain cooling of the surface as the surface approached the temperature of the clouds. However, the low frequency of occurrence of ice PSCs means that any moderation of surface temperature evolution would be intermittent and infrequent.

We next consider the thermal emission balance of the polar snow surface under clear night skies as temperatures approach the lowest values (Figure S6). Radiance of the snow surface upward is essentially that of a blackbody (ε = 0.997 to 0.999). At surface snow temperatures above about −55 °C, much of the spectrum of thermal emission is within the broad high-transmittance range for the atmosphere between 7 and 13-μm wavelength (−55 °C peak emission is 13.3 μm). At temperatures of −75 °C and below, the peak emission shifts into a CO_2 absorption band between 13.5 and 17.5-μ wavelength (−75 °C peak emission is 14.6 μm; −95 °C peak is 16.3 μm). In this range, much of the emitted thermal radiation from the surface is absorbed by CO_2 in the near-surface atmosphere and reradiated downward. This slows the rate of surface cooling, as observed in the time series LST data in Figures 2 and S4.

Under typical conditions, water vapor in the air column absorbs radiation at wavelengths longer than the CO_2 band (i.e., in the far infrared). However, during much of the polar winter, the East Antarctic Plateau experiences extremely low levels of precipitable water, generally below 0.5 mm (Thomas et al., 2011) and in the East Antarctic ice divide region, often below 0.2 mm, with periods as low as 0.04 mm (Yang et al., 2010). These periods of atmospheric clarity and extremely dry air permit further radiative emission loss from the 17.5 μm and higher wavelength regions. Models of atmospheric transmissivity and emissivity under these conditions (e.g., Berk et al., 2014) show that clear-air downwelling radiation is strongly dependent on water vapor. Examining several model runs of MODTRAN® using conditions similar to those observed for the ultracold sites (Figure S6) shows that net differences in upwelling and downwelling radiation become very small, for example, 10.4 W/m^2 for −95 °C near-surface air temperature (with an air column temperature profile similar to the annual minimum at South Pole), −95 °C surface snow temperature, and ~0.1-mm precipitable water (10 atm cm).

A model of the subsurface snow and firn temperature profile, snow surface emissivity, and snow thermal conductivity under these emission conditions (adapted from Muto et al., 2011), using an initial snow surface temperature of −75 °C, showed that the surface temperature reaches −97 °C after 5 days. However, at that point, cooling rates of the surface are ~0.02 °C/hr and decreasing with time, essentially setting a low temperature limit. Higher levels of water vapor in the air column prevent the surface from reaching −95 °C in the model, even with low air temperatures. Both downwelling radiation and heat conduction from the upper firn limit the pace of surface cooling.

5. Conclusion

A broad area of the upper East Antarctic ice divide regularly experiences surface snow temperatures of −90 °C and below, with isolated topographic lows along the uppermost south side of the divide crest reaching observed temperatures (recorded in MODIS LST data) of −98.0 to −98.6 ± 1 °C. Comparison with the nearest AWS and station data implies near-surface (2 m) air temperatures of −94 ± 4 °C at the ultracold sites after applying estimated corrections for MODIS LST bias and near-surface air temperature gradients. Ultralow temperature events in Antarctica are more common during strong circumpolar circulation periods (and thus positive SAM index).

Our conceptual model for the record-setting surface temperatures (Figure S7) starts with strong radiative cooling of the snow surface and a strong surface-based temperature inversion, leading to downhill drainage of a near-surface air layer. The cold air collects in local topographic lows, allowing the surface snow in these sites to cool still further by reducing the advection (downward or laterally) of less chilled air. We suspect that the near-surface air temperature gradient may be less steep within the topographic lows, making it likely that these record low snow temperatures underlie record cold air at 2 m. Adjacent higher-elevation dome and flank areas of the ice surface are not able to cool as much because divergent drainage of the near-surface air leads to subsidence, exposing the surface to warmer air from higher in the inversion layer. Cooling proceeds as long as clear atmospheric and low wind speed conditions remain, but cooling to ~−98 °C requires light winds, clear skies, and very low atmospheric water vapor (~0.1-mm precipitable water) to persist for several days. Surface snow cooling rates are near-zero (~0.02 °C hr^{-1}) as this limit is approached.

The radiative processes that control record low surface and air temperatures, and the changing composition of the atmosphere, imply that in the future, we may see fewer extreme low temperature events. This is due to

the ongoing increase in gases such as CO_2 and to increased water vapor in the Antarctic atmosphere as a secondary effect.

Acknowledgments
Land surface thermal emission data used in this study (MOD11 and MYD11 and Collection 6) are available from, for example, https://modis.gsfc.nasa.gov/data/dataprod/mod11.php. Weather station data used here are available from Institute for Marine and Atmospheric Research, Physics and Astronomy Department, Utrecht University, the National Center for Environmental Information, and the Australian Antarctic Data Centre at https://data.aad.gov.au/metadata/records/DomeA_AWS. Landsat imagery is available from https://earthexplorer.usgs.gov. This research was supported by USGS award G12PC00066 and NASA awards NNX14AM54G and NNX14AH79G to T.A.S. and NSF ANT-154335 to M.A.L. We thank Craig Kulessa and Michael Ashley for informative discussions based on their data from Ridge A in East Antarctica.

References

Adolph, A. C., Albert, M. R., & Hall, D. K. (2018). Near-surface temperature inversion during summer at Summit, Greenland, and its relation to MODIS-derived surface temperature. *The Cryosphere*, *12*(3), 907–920. https://doi.org/10.5194/tc-12-907-2018

Albert, M. R., Shuman, C. A., Courville, Z., Bauer, R., Fahnestock, M. A., & Scambos, T. (2004). Extreme firn metamorphism: Impact of decades of vapour transport on near-surface firn at a low-accumulation glazed site on the East Antarctic Plateau. *Annals of Glaciolgy*, *39*(1), 73–78. https://doi.org/10.3189/172756404781814041

Bamber, J. L., Gomez-Dans, J. L., & Griggs, J. A. (2009). A new 1 km digital elevation model of the Antarctic derived from combined satellite radar and laser data—Part 1: Data and methods. *The Cryosphere*, *3*(1), 101–111. https://doi.org/10.5194/tc-3-101-2009

Bell, R. E., Ferraccioli, F., Creyts, T. T., Braaten, D., Corr, H., Das, I., et al. (2011). Widespread persistent thickening of the East Antarctic Ice Sheet by freezing from the base. *Science*, *331*(6024), 1592–1595. https://doi.org/10.1126/science.1200109

Berk, A., Conforti, P., Kennett, R., Perkins, T., Hawes, F., & van den Bosch, J. (2014). MODTRAN® 6: A major upgrade of the MODTRAN® radiative transfer code. In Hyperspectral Image and Signal Processing: Evolution in Remote Sensing (WHISPERS), 2014 6th Workshop on (1–4). IEEE. https://doi.org/10.1109/WHISPERS.2014.8077573

Campbell, G. G., Pope, A., Lazzara, M., & Scambos, T. A. (2013). The coldest place on Earth: −90°C and below in East Antarctica from Landsat 8 and other thermal sensors, Abstract C21D-0678 presented at the 2013 Fall Meeting, AGU, San Francisco, CA, 9–13 Dec.

Dozier, J., & Warren, S. G. (1982). Effect of viewing angle on the infrared brightness temperature of snow. *Water Resources Research*, *18*(5), 1424–1434. https://doi.org/10.1029/WR018i005p01424

Gerace, A., & Montanaro, M. (2017). Derivation and validation of the stray light correction algorithm for the Thermal Infrared Sensor onboard Landsat 8. *Remote Sensing of Environment*, *191*, 246–257. https://doi.org/10.1016/j.rse.2017.01.029

Gladkova, I., Shahriar, F., Grossberg, M., Frey, F., & Menzel, W. P. (2013). Impact of the Aqua MODIS band 6 restoration on cloud/snow discrimination. *Journal of Atmospheric and Oceanic Technology*, *30*(12), 2712–2719. https://doi.org/10.1175/JTECH-D-13-00066.1

Hall, D., Box, J. E., Casey, K. A., Hook, S. J., & Shuman, C. A. (2008). Comparison of satellite-derived and in situ observations of ice and snow surface temperatures over Greenland. *Remote Sensing of Environment*, *112*(10). https://doi.org/10.1016/j.rse.2008.05.007

Haran, T. M., Bohlander, J. C., Scambos, T. A., Painter, T., & Fahnestock, M. (2014). MODIS mosaic of Antarctica 2008–2009 (MOA2009) image map, Version 1. Boulder, Colorado USA. National Snow and Ice Data Center. https://doi.org/10.7265/N5ZK5DM5

Hudson, S. R., & Brandt, R. E. (2005). A look at the surface-based temperature inversion on the Antarctic Plateau. *Journal of Climate*, *18*(11), 1673–1696. https://doi.org/10.1175/JCLI3360.1

King, J. C., Anderson, P., Smith, M., & Mobbs, S. (1996). The surface energy and mass balance at Halley, Antarctica during winter. *Journal of Geophysical Research*, *101*(D14), 19,119–19,128. https://doi.org/10.1029/96JD01714

Marshall, G., & National Center for Atmospheric Research Staff (Eds.). Last modified 10 Jun (2016). "The climate data guide: Marshall Southern Annular Mode (SAM) index (station-based)." Retrieved from https://climatedataguide.ucar.edu/climate-data/marshall-southern-annular-mode-sam-index-station-based

Marshall, G. J. (2003). Trends in the Southern Annular Mode from observations and reanalyses. *Journal of Climate*, *16*(24), 4134–4143. https://doi.org/10.1175/1520-0442(2003)016

Mildrexler, D. J., Zhao, M., & Running, S. W. (2006). Where are the hottest spots on Earth? *Eos*, *87*(43), 461–467. https://doi.org/10.1029/2006EO430002

Muto, A., Scambos, T. A., Steffen, K., Slater, A. G., & Clow, G. D. (2011). Recent surface temperature trends in the interior of East Antarctica from borehole firn temperature measurements and geophysical inverse methods. *Geophysical Research Letters*, *38*, L15502. https://doi.org/10.1029/2011GL048086

Parish, T. R., & Bromwich, D. H. (1987). The surface windfield over the Antarctic ice sheets. *Nature*, *328*(6125), 51–54. https://doi.org/10.1038/328051a0

Phillpot, H. R., & Zillman, J. W. (1970). The surface temperature inversion over the Antarctic continent. *Journal of Geophysical Research*, *75*(21), 4161–4169. https://doi.org/10.1029/JC075i021p04161

Pitts, M. C., & Poole, L. R. (2015). CALIPSO polar stratospheric cloud observations from 2006–2015; (2015), European Geosciences Union General Assembly; 12-17 Apr. 2015; Vienna; Austria, Abstract AS3.12–5899; NASA Technical Report NF1676L-21147.

Pitts, M. C., Poole, L. R., & Thomason, L. W. (2009). CALIPSO polar stratospheric cloud observations: Second-generation detection algorithm and composition discrimination. *Atmospheric Chemical Physics*, *9*(19), 7577–7589. https://doi.org/10.5194/acp-9-7577-2009

Roy, D. P., Wulder, M. A., Loveland, T. R., Woodcock, C. E., Allen, R. G., Anderson, M. C., et al. (2014). Landsat-8: Science and product vision for terrestrial global change research. *Remote Sensing of Environment*, *145*, 154–172. https://doi.org/10.1016/j.rse.2014.02.001

Salisbury, J., D'Aria, D. M., & Wald, A. (1994). Measurements of thermal infrared spectral reflectance of frost, snow, and ice. *Journal of Geophysical Research*, *99*(B12), 24,235–24,240. https://doi.org/10.1029/94JB00579

Scambos, T. A., Haran, T. M., & Massom, R. A. (2006). Validation of AVHRR and MODIS ice surface temperature products using in situ radiometers. *Annals of Glaciology*, *44*(1), 345–351. https://doi.org/10.3189/172756406781811457

Schwerdtfeger, W. (1970). The climate of the Antarctic. *World Survey of Climatology*, *14*, 253–355.

Shuman, C. A., Hall, D. K., DiGirolamo, N. E., Mefford, T. K., & Schnaubelt, M. J. (2014). Comparison of near-surface air temperatures and MODIS ice surface temperatures at summit, Greenland (2008-13). *Journal of Applied Meteorology and Climatology*, *53*(9), 2171–2180. https://doi.org/10.1175/JAMC-D-14-0023.1

Stepanova, N. A. (1963). The world's lowest temperature record. *Weatherwise*, *16*(6), 268–269. https://doi.org/10.1080/00431672.1963.9930038

Thomas, I. D., King, M. A., Clarke, P. J., & Penna, N. T. (2011). Precipitable water vapor estimates from homogeneously reprocessed GPS data: An intertechnique comparison in Antarctica. *Journal of Geophysical Research*, *116*, D04107. https://doi.org/10.1029/2010JD013889

Turner, J., Anderson, P., Lachlan-Cope, T., Colwell, S., Phillips, T., Kirchgaessner, A., et al. (2009). Record low surface air temperature at Vostok station, Antarctica. *Journal of Geophysical Research*, *114*, D24102. https://doi.org/10.1029/2009JD012104

Van den Broeke, M. R., & van Lipzig, N. P. M. (2003). Factors controlling the near-surface wind field in Antarctica. *Monthly Weather Review*, *131*(4), 733–743. https://doi.org/10.1175/1520-0493(2003)131%3C0733:FCTNSW%3E2.0.CO;2

Wan, Z. (2006). MODIS Land Surface Temperature products user's guide". Santa Barbara, CA. Retrieved from http://www.icess.ucsb.edu/modis/LstUsrGuide_v5/MODIS_LST_products_Users_guide.pdf

Wan, Z. (2014). New refinements and validation of the collection-6 MODIS land surface temperature/emissivity product. *Remote Sensing of Environment*, *140*, 36–45. https://doi.org/10.1016/j.rse.2013.08.027

Wang, X., & Key, J. (2005). Arctic surface, cloud, and radiation properties based on the AVHRR Polar Pathfinder data set. Part I: Recent trends. *Journal of Climate*, *18*(14), 2558–2574. https://doi.org/10.1175/JCLI3438.1

Wang, Y., Wang, M., & Zhao, J. (2013). A comparison of MODIS LST retrievals with in situ observations from AWS over the Lambert Glacier basin, East Antarctica. *International Journal of Geosciences*, *04*(03), 611–617. https://doi.org/10.4236/ijg.2013.43056

Weller, G., & Schwerdtfeger, P. (1977). Thermal properties and heat transfer processes of low-temperature snow. In P. Antarctica, et al. (Eds.), *Meteorological studies at plateau station* (pp. 27–34). Washington, DC: American Geophysical Union. https://doi.org/10.1002/9781118664872.ch3

Yang, H., Kulesa, C. A., Walker, C. K., Tothill, N. F., Yang, J., Ashley, M. C., et al. (2010). Exceptional terahertz transparency and stability above Dome A, Antarctica. *Publications of the Astronomical Society of the Pacific*, *122*(890), 490–494. https://doi.org/10.1086/652276